

# Searching for SUSY in all hadronic final states with the $\alpha_T$ variable

Bryn Mathias  
Imperial College London

Supervisor: Dr Alex Tapper

## Abstract

1

2

This is a thesis.

## Declaration

There are many like it.

Author

## Acknowledgements

1

2

Thanks.

# Contents

<b>1</b>	<b>Introduction</b>	<b>7</b>
<b>2</b>	<b>Theory</b>	<b>8</b>
<b>3</b>	<b>The CMS detector</b>	<b>9</b>
3.1	The High Level Trigger System . . . . .	9
<b>4</b>	<b>Offline Object Reconstruction and Identification.</b>	<b>10</b>
4.1	Hadronic Jets. . . . .	10
4.2	Electrons. . . . .	10
4.3	Muons. . . . .	10
4.4	Photons. . . . .	10
4.5	Noise cleaning. . . . .	11
<b>5</b>	<b>Level One Calorimeter Trigger</b>	<b>12</b>
5.1	Level-1 Trigger Jet Algorithm [10] . . . . .	13
5.2	Level-1 Trigger Performance . . . . .	15
5.3	Level-1 Trigger Pile-up Mitigation . . . . .	23
5.3.1	Effect on trigger efficiency . . . . .	25
5.3.2	Summary . . . . .	27
<b>6</b>	<b>High level triggers for the <math>\alpha_T</math> analysis.</b>	<b>29</b>
<b>7</b>	<b>The <math>\alpha_T</math> analysis</b>	<b>30</b>
7.1	The Problem . . . . .	30
7.2	The $\alpha_T$ variable. . . . .	31
7.3	Event selection . . . . .	32
7.4	High Level triggers for the $\alpha_T$ analysis . . . . .	35
7.5	2011 Trigger . . . . .	36
7.5.1	Trigger efficiency measurement . . . . .	37

1	7.6 Electro-Weak background prediction . . . . .	37
2	<b>8 Conclusion</b>	<b>39</b>
3	<b>Bibliography</b>	<b>41</b>
4		

# Chapter 1

## Introduction

**The accelerator and detectors** The Large Hadron Collider (LHC) [3] is a proton-proton collider which is situated in the Large Electron Positron (LEP) tunnel approximately 100 m under the franco-swiss border. Design center of mass energy is 14 TeV with an instantaneous luminosity of  $1 \times 10^{34} \text{cm}^{-2}\text{s}^{-1}$ . However during 2011 the center of mass energy was 7 TeV and the maximum luminosity was  $5 \times 10^{33} \text{cm}^{-2}\text{s}^{-1}$ . To achieve this high energy and high beam current the LHC uses superconducting niobium-titanium magnets, cooled to a temperature of 1.8 Kelvin, that produce a maximum field strength of 8.36 Tesla.

**TODO: we might well need some more stuff about the LHC its self in here!**

Situated around the LHC ring are four detectors, two general detectors ATLAS [1] and CMS (see Chapter 3 for a detailed discussion of the CMS detector) [9][13] which are designed to measure the standard model to high precision and search for new physics. The LHC beauty experiment [11] is designed to study at previously unattainable precision the decays of heavy quark flavors, both to measure the standard model couplings and to search for beyond the standard model (BSM) physical processes. Finally the ALICE [2] experiment is designed to run when the LHC is running in it's secondary mode where rather than proton bunches, lead ions are collided, in an effort to study the quark-gluon plasma.

**New physics** Whilst the theory of the standard model and of new physics models will be discussed in chapter 2 it is prudent to discuss the observable features of these models with regard to design requirements for the general purpose detectors.

## Chapter 2

### <sub>1</sub> Theory



# **Chapter 3**

## **<sub>1</sub> The CMS detector**

### **<sub>2</sub> 3.1 The High Level Trigger System**

# Chapter 4

## 1 Offline Object Reconstruction and 2 Identification.

### 3 4.1 Hadronic Jets.

4 AK5 calo jets – explanation of the jet algos. How they are clustered at CMS. No need to  
5 mention PF? (we don't use it so why bother). Energy resolution, Jet energy corrections,  
6 ID. 2011 note

### 7 4.2 Electrons.

8 GSF elections - ID, use tracking. Veto on elections. 2011 note

### 9 4.3 Muons.

10 GPT muons - exact ID's, reconstruction methods. both veto and used to collect the  
11 control sample. 2011 note

### 12 4.4 Photons.

13 Veto and control sample - noise and spike cleaning 2011 note

## <sup>1</sup> 4.5 Noise cleaning.

<sup>2</sup> Dead ecal sections. monsters. Trackless events. 2011 note.

# Chapter 5

## Level One Calorimeter Trigger

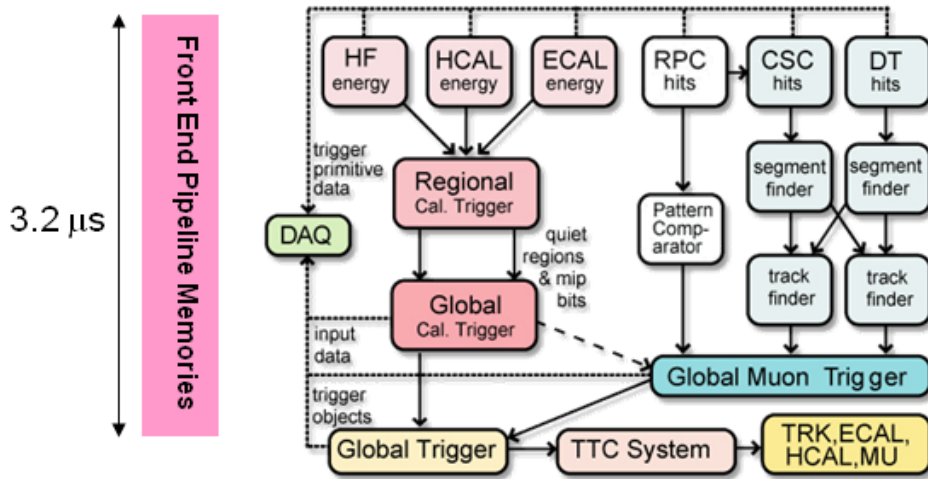


Figure 5.1: The CMS Level-1 Trigger system

The CMS Level-1 trigger system[6] is a pipelined dead-timeless system based on custom-built electronics. The Level-1 trigger is a combination of several sub systems, which are interconnected as depicted in Figure 5.1.

Coarse grain information from the electro-magnetic, hadronic and forward calorimeters is processed by the Regional Calorimeter Trigger (RCT), this is then passed to the Global Calorimeter Trigger (GCT) where the coarse grain information is clustered in to physics objects, these objects are then passed to the Global Trigger where the Level-1 accept decision is made. Due to the limited size of the pipe line this Level-1 accept must be issued within 4.0 μs.

The objects passed from the GCT to the GT include electro-magnetic objects, both electrons and photons as due to the lack of tracking information at the Level-1 trigger these objects are indistinguishable, jets and energy sums.

The RCT generates up to 72 isolated and non-isolated electro-magnetic objects, these are sorted by rank, which is equivalent to transverse energy  $E_T$ . The four highest ranked electro-magnetic objects are then passed via the GCT to the GT at an equivalent data rate of 29 Gbs<sup>-1</sup> per type.

Hadronic objects under go two clustering steps. First the transverse energy sums of the ECAL and corresponding HCAL towers are calculated, the towers are then summed in to 4×4 trigger regions, these are passed to the GCT at a data rate of 172.8 Gbs<sup>-1</sup>. These trigger regions are clustered in to jet candidates by the GCT and ranked. The jets are then sub-divided in the categories depending on their pseudo-rapidity and the result of  $\tau$  identification.

Energy sums come in two forms, the total transverse energy  $E_T$  which is the scalar sum of all transverse energies and the total jet transverse energy  $H_T$  which is calculated as the scalar sum of all jets above some programable threshold.

The missing energy equivalents of these  $\cancel{E}_T$  and  $\cancel{H}_T$  are formed from the negative vector sum of the objects considered for the transverse sums.

## 5.1 Level-1 Trigger Jet Algorithm [10]

The CMS detector can be un-rolled in the  $\phi$  direction to form a rectangular grid of the 396 calorimeter regions, connected along the  $\phi$  edge. The rectangle is formed from 18  $\phi$  divisions (from  $-180^\circ < \phi \leq 180^\circ$ ) and 22  $\eta$  divisions ( from  $-5 < \eta < 5$ ). Each  $\phi$  division corresponds to  $20^\circ$ . The  $\eta$  divisions correspond to  $\Delta\eta = 0.5$  in the forward calorimeters and to  $\Delta\eta \approx 0.348$  in the barrel. A pictorial representation of this can be seen in figure 5.3.

A jet candidate is created if the sum of the ECAL and HCAL energies of the central calorimeter region has an energy deposit larger than all of its neighbours, as shown in figure 5.2 The jet is centred at this region where  $p_T^{central} > p_T^{surrounding}$  and the transverse energies of the surrounding regions are summed in to the central region. The jet is then classified as a  $\tau$  jet if  $|\eta| < 3.0$  and none of the  $\tau$  veto bits are set. If any  $\tau$  vetoes are set the jet is classified as a central jet. The jet is classified as forward if  $3.0 < |\eta| < 5.0$

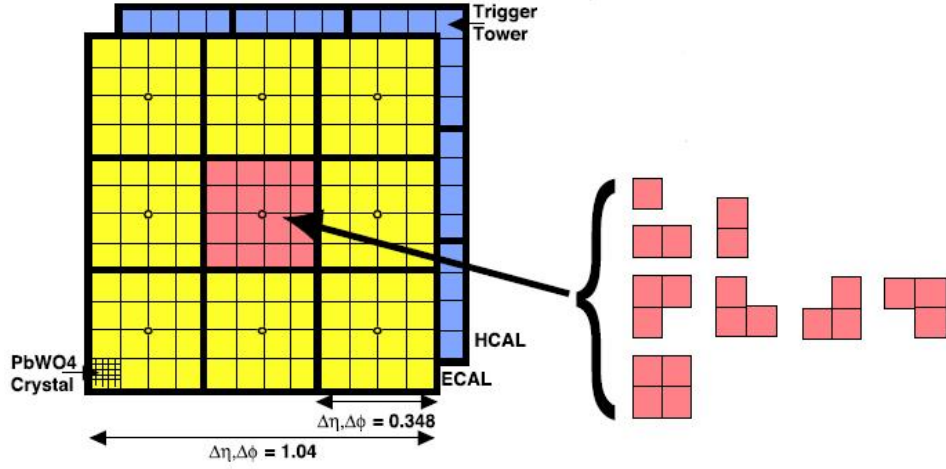


**Figure 5.2:** The  $3 \times 3$  jet-finder window at Level-1. Each cell represents a trigger tower, which is the sum of the HCAL and ECAL transverse energies. The  $\tau$ -jet veto patterns are shown to the right.

The  $\tau$ -vetoes are set by the RCT depending on whether or not the energy depositions in up to four contiguous trigger towers are below a programmable fraction of the regional  $E_T$  as shown in Figure 5.2.

It is possible to apply separate jet energy corrections to each of the sub categories of GCT jets, however at current the same  $E_T$  and  $\eta$  dependant corrections are used for all three jet types.

In order to reduce the total data duplicated and shared between the jet finders the GCT employs a pre-clustering algorithm, which involves 18 jet finders operating simultaneously over the whole detector. These jet finders then only share information with neighbouring regions when the clustered jets are found. Figure 5.3 shows the boundaries between which the jet finders operate, these map naturally on to one RCT crate per jet finder. A maximum of 3 jets can be found on each of the  $\phi$  strips acted on by the jet finders, this gives a maximum of 108 jets per event. In order to preserve continuity across the  $\eta = 0$  boundary, the two adjacent trigger regions are shared between the jet finders.

An example of the jet finding is shown in Figure 5.4. The first step is to create a  $2 \times 3$  mini cluster around any local maxima found in the  $12 \times 2$  strip. Equality statements are imposed so that the energy of the central cell is greater than its neighbours in some directions and greater than or equal to the neighbours other directions to enforce a gap of at least one trigger region in both  $\eta$  and  $\phi$  between the centres of the clustered jets.

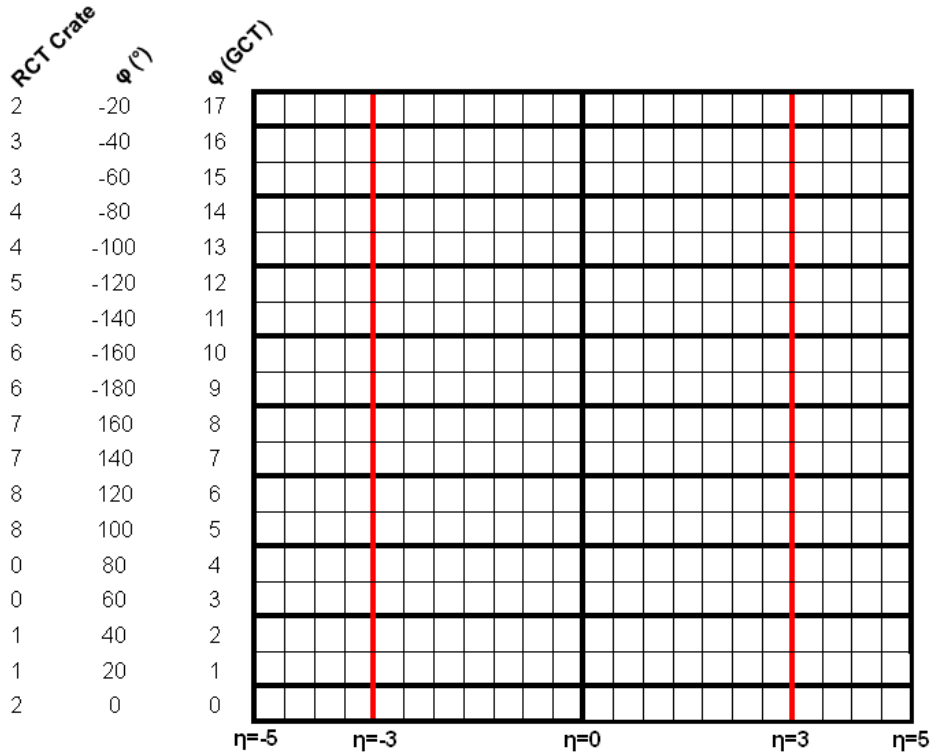


**Figure 5.3:** The calorimeter map that the  $3 \times 3$  jet-finder operates over is made up for 396 calorimeter regions, each jet finder is mapped on to an RCT crate which is composed of an  $11 \times 2$  strip of these regions. RCT crate labels are shown for negative  $\eta$  only.

1 In the second step the jet finder transfers the three largest mini clusters on a given  
2  $\phi$  strip to the closest  $\phi$  strip on the neighbouring jet finder. These are then compared  
3 against the existing mini clusters in that  $\phi$  strip, those that are adjacent or diagonally  
4 adjacent to a larger mini cluster are removed. The inequality statements are then  
5 reimposed to prevent problems with clusters having the same energies. In the final stages  
6 the mini clusters have their three adjacent regions summed in to produce a  $3 \times 3$  jet  
7 cluster. Finally the four highest ranked jets are corrected and passed to the GT.

## 8 5.2 Level-1 Trigger Performance

9 During the start of data taking in 2010, no Jet Energy Corrections (JEC's) were applied  
10 in the Level-1 trigger. This gave a relatively slow turn on in terms of offline hadronic  
11 objects. During the winter shut down of the LHC between the 2010 and 2011 running  
12 periods a set of Level-1 JEC's were developed. These corrections used a peicewise cubic

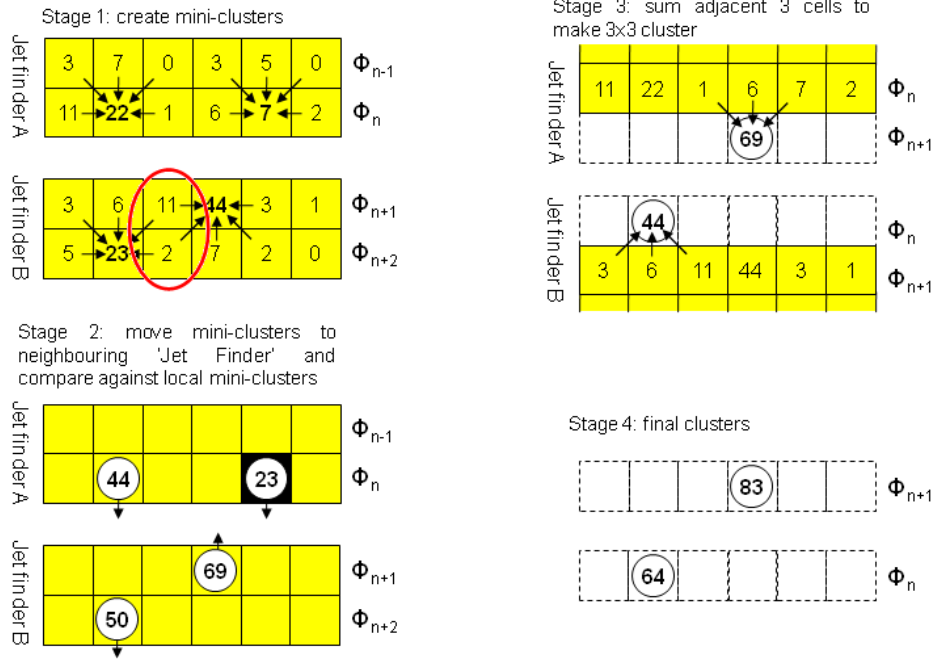


**Figure 5.4:** The Level-1 jet clustering method, six cells in  $\eta$  are shown. An example of overlapping jets is shown

1 form for the interpolation function used to correct the jet energy dependant on it's  
 2 uncorrected  $E_T$  and  $\eta$  values. However as can be seen in Figure 5.5 these corrections  
 3 were only applied to jets with a raw energy below 130 GeV, the secondary lobe shows  
 4 those objects that do not have their energy corrected.

5 To overcome this a new set of corrections were derived using a well established tool  
 6 for producing offline corrections, **REFERENCE TO tapper-001** here using the same  
 7 functional form that was derived for correcting particle flow jets. **REFERENCE TO**  
 8 **PF HERE** In this section we discuss the performance of both sets of Level-1 JEC's and  
 9 the performance of the energy sum triggers  $H_T$ ,  $\cancel{H}_T$ , and  $\cancel{E}_T$ , the performance of which  
 10 are not effected by the application of jet energy corrections at the Level-1 trigger due  
 11 to the quantities being built from the internal GCT jets before they pass though the  
 12 corrections look up table. The performance is studied under both low pile up conditions  
 13 where the mean peak pile up  $\langle PU \rangle$  is 16 primary vertices and under high pile up  
 14 conditions where  $\langle PU \rangle$  is 36 primary vertices.

15 To measure the performance of the Level-1 single jet triggers we assume that the  
 16 leading offline corrected anti- $k_t(0.5)$  calorimeter jet is the jet that triggered the event.  
 17 We then match this offline jet to the closest Level-1 jet in  $\Delta R$ , where for there to be a  
 18 match  $\Delta R < 0.5$  is required. For this match central,  $\tau$  and forward jets are considered.



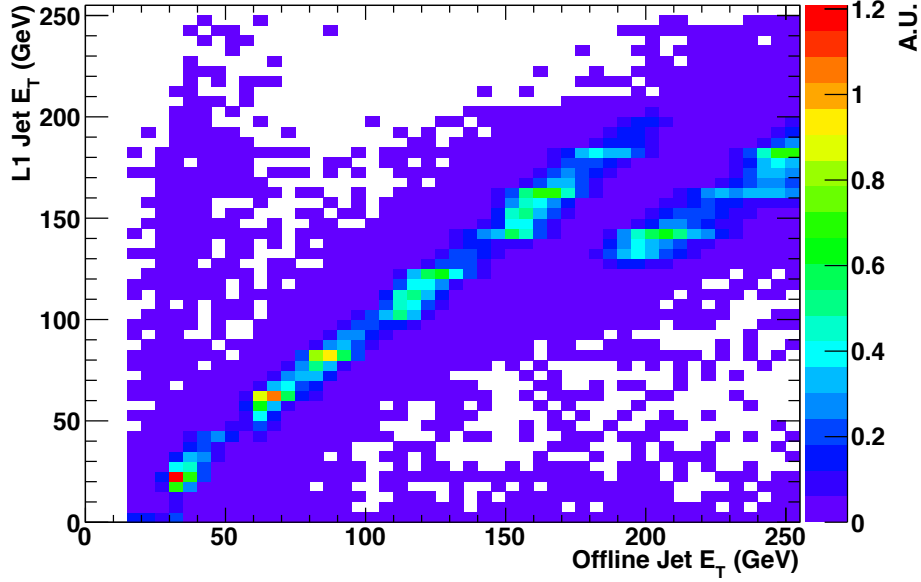


**Figure 5.5:** Correlation between offline corrected jet energy and Level-1 corrected jet energy for matched jets. The discontinuity shows where the Level-1 jet corrections do not alter the raw energy of the jet.

Events where the recorded Level-1 energy is set to the overflow bit, meaning they have more than 254 GeV of  $E_T$  measured at Level-1 are ignored.

To collect an unbiased sample in which to measure the performance, two methods are used; the first is to require a Minimum Bias trigger, which is triggered by beam induced activity in the CMS detector. However due to the nature of these collisions the number of events with high energy interactions is low and the prescale applied to this trigger further reduces the sample size. However this method does produce the least bias. The second method is to trigger an object that does not deposit significant energy in the calorimeter systems, in this case we choose the muon trigger with the lowest unprescaled  $p_T$  threshold. The muon trigger is chosen with some loose isolation requirements to make sure it does not overlap with a jet, causing a discrepancy in the measure of the calorimetric energy. The sample has a higher number of events due to the large amount of bandwidth given to the single object muon triggers in CMS. The use of a muon trigger also serves to increase the precision of the measurement of the Level-1 missing energy trigger as the muons are not seen by the calorimeter system the  $\cancel{E}_T$  sample is enriched.

Figure 5.6 shows the performance of the piecewise cubic corrections (PWC) and the performance of the new corrections. The data was taken with the PWC enabled in the

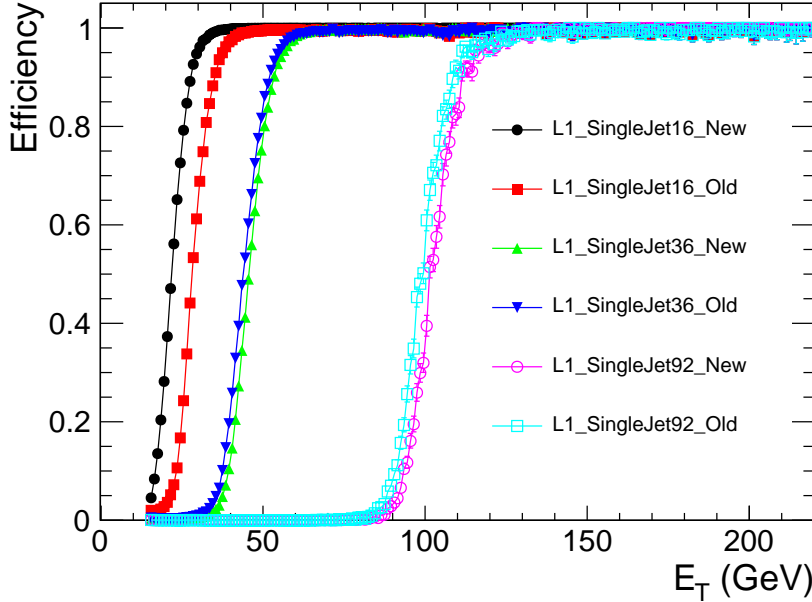


**Figure 5.6:** Comparison of the performance of L1\_SingleJet16, L1\_SingleJet36 and L1\_SingleJet92, when using the piecewise cubic corrections and using the new correction scheme. The difference in performance of the two is negligible above 36 GeV.

GCT hardware. The updated corrections were emulated in the bitwise reproduction of the GCT. This made an event by event comparison possible. At low  $E_T$  the new corrections turn on before the PWC corrections, if the new corrections were applied on with no change to the trigger menu, the Level-1 trigger rate would rise. At a threshold of 36 GeV and higher the performance of the two correction schemes is very similar. Due to the small change in observed performance and the ability to correct raw energies above 130 GeV, the new corrections were deployed online at the start of Run2011B and are still online at the end of data taking in 2012.

The performance of the updated corrections was then measured with data taken with the corrections applied in the GCT hardware. The reference sample was taken with the HLT\_IsoMu24\_v\* high level muon trigger. The performance of three example triggers is shown in Figure 5.7. The data collected and represented in Figure 5.7 has a peak mean pile up ( $\langle PU \rangle$ ) of 16 interactions, this is higher than the  $\langle PU \rangle$  of approximately 8-10 present in Run2011A, on which the previous comparison was performed. The observed difference in the performance of the Level-1 single jet triggers as a function of pile up is a cause for concern when data taking is underway at the LHC's design luminosity, where  $\langle PU \rangle$  is  $>36$  at an instantaneous luminosity of  $1 \times 10^{34} \text{ cm}^{-2} \text{ s}^{-1}$ .

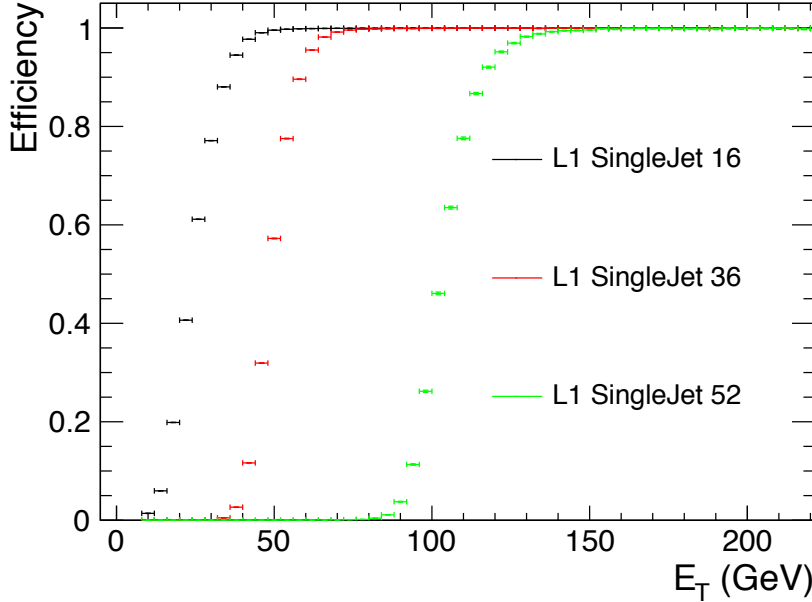


**Figure 5.7:** Performance measurements of L1\_SingleJet16, L1\_SingleJet36 and L1\_SingleJet92, when using the new correction scheme deployed in the GCT hardware. The performance is slightly worse than that of the emulated triggers due to a change in pile up conditions between the two data taking periods.

1 The instantaneous luminosity in 2012 was predicted to be  $5 \times 10^{33} \text{cm}^{-27} \text{s}^{-1}$ , with  
 2  $\langle PU \rangle \approx 32$ . In order to study the effect on the trigger rate and efficiency a high pile  
 3 up, low instantaneous luminosity, LHC fill was taken in 2011.

4 The Level-1 single jet performance was studied in this run in terms of two offline  
 5 object definitions. The first was the standard anti- $k_t(0.5)$  calorimeter jet reconstruction,  
 6 the second was a set of anti- $k_t(0.5)$  calorimeter jets which were corrected for pile up using  
 7 the fastjet correction algorithm, **cite fast jet** which is further detailed in Section 4. The  
 8 fast-jet corrections remove the energy deposited by the secondary interactions from the  
 9 objects which are expected to come from the primary hard interaction, thus removing  
 10 energy from the offline jets. The effect of these pile up corrections on the Level-1 trigger  
 11 performance is first studied under conditions with  $\langle PU \rangle$  of 16, the performance of  
 12 which has already been measured with respect to non pile up corrected offline objects,  
 13 as a sanity check. The results are shown in Figure 5.8, the performance is measured  
 14 with respect to HLT\_IsoMu24\_v\*, in terms of both pile up corrected and standard offline  
 15 objects. As expected the performance in the two cases is very similar. The same  
 16 comparison is shown for  $H_T$  in Figure 5.9, where the effect of the fastjet corrections is

more pronounced due to the sum over jets. The difference between the turn on points for the two offline quantities is on the order of 10 GeV under low pile up conditions.

Due to the high pile up fill being a specialised fill with low instantaneous luminosity, the high level trigger paths were disabled, instead Level-1 trigger pass through paths were utilised to take the data. The Level-1 single muon pass through trigger is used to collect the reference sample. Otherwise the same analysis method is common between the two data sets. Figure 5.10 shows the difference in turn on for three example Level-1 single jet triggers when using standard calorimeter jets and fastjet corrected calorimeter jets. In the high pile up conditions the switch to offline jets that are corrected for pile up shifts the turn on point to lower values of  $E_T$ , the magnitude of this effect reduces as the Level-1 trigger threshold raises. This implies that the same offline performance as seen in the low pile up conditions can be achieved by using the pile up corrected offline objects and raising the Level-1 single jet trigger thresholds.

Figure 5.11 shows the same high pile up comparison, but for the Level-1  $H_T$  triggers. Due to the size of the sample the precision of this measurement is low. However the same trend of a shift to lower  $H_T$  values of the turn on point of the Level-1 triggers when using pile up corrected offline objects is observed. This again implies that the Level-1  $H_T$  trigger thresholds can be raised whilst preserving the same offline performance as during the low pile up conditions.

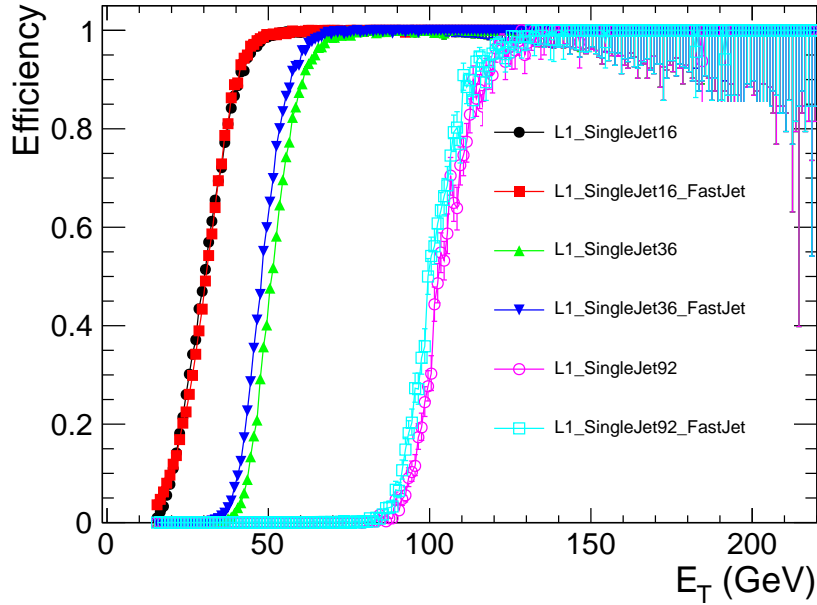


**Figure 5.8:** Comparison of the performance of L1\_SingleJet16, L1\_SingleJet36 and L1\_SingleJet92 triggers. Where  $\langle PU \rangle = 16$ . For two offline reconstruction methods, standard anti- $k_t(0.5)$  calorimeter jets and pile up corrected anti- $k_t(0.5)$  calorimeter jets.

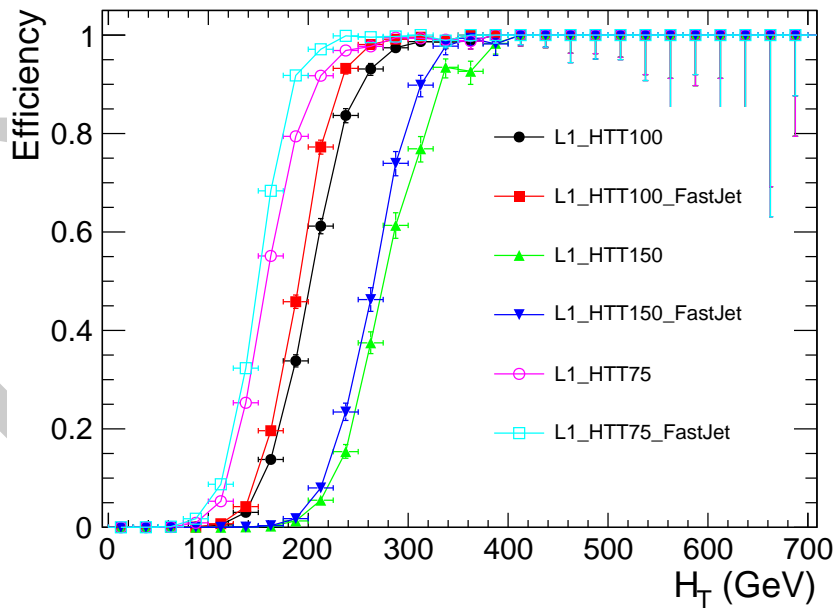


**Figure 5.9:** Comparison of the performance of L1\_HTT75, L1\_HTT100 and L1\_HTT150 triggers. Where  $\langle PU \rangle = 16$ . For two offline reconstruction methods, standard anti- $k_t(0.5)$  calorimeter jets and pile up corrected anti- $k_t(0.5)$  calorimeter jets.

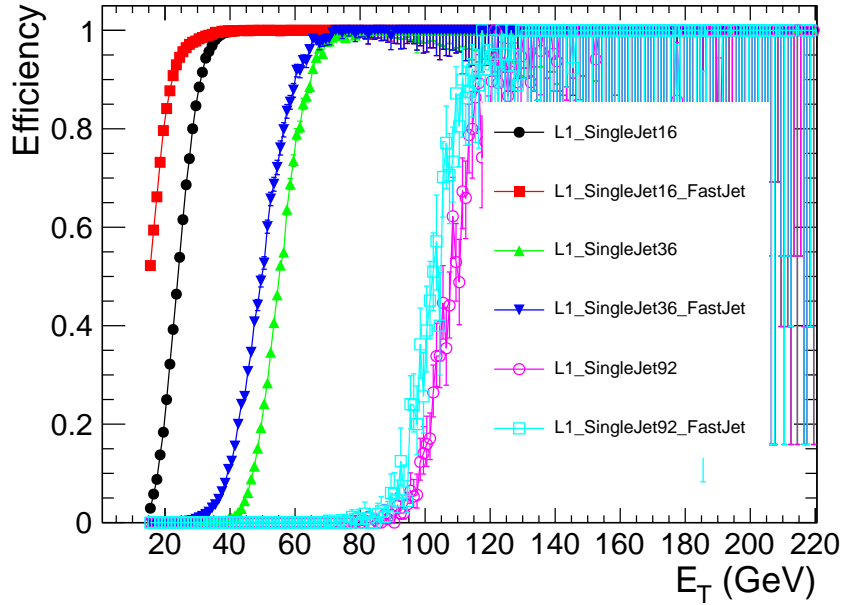


**Figure 5.10:** Comparison of the performance of L1\_SingleJet16, L1\_SingleJet36 and L1\_SingleJet92 triggers. Where  $\langle PU \rangle = 36$ . For two offline reconstruction methods, standard anti- $k_t(0.5)$  calorimeter jets and pile up corrected anti- $k_t(0.5)$  calorimeter jets.

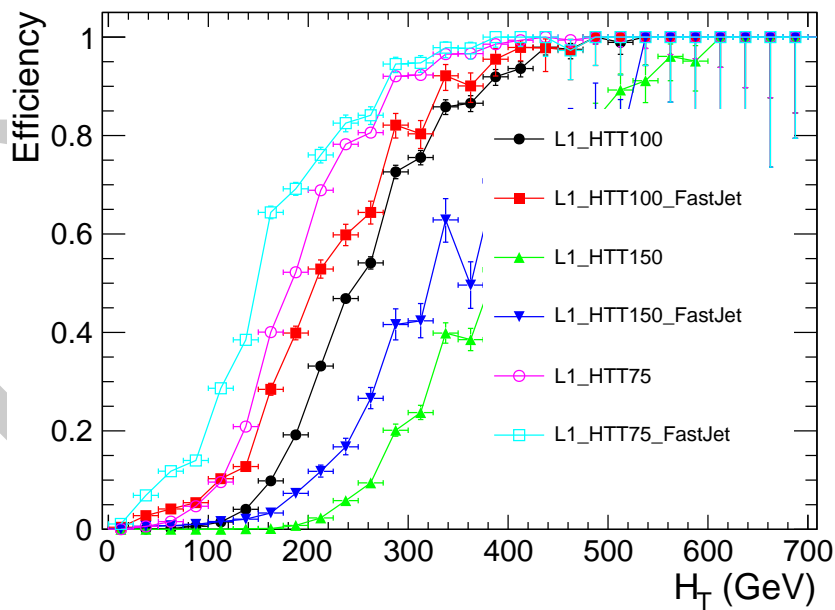


**Figure 5.11:** Comparison of the performance of L1\_HTT75, L1\_HTT100 and L1\_HTT150 triggers. Where  $\langle PU \rangle = 36$ . For two offline reconstruction methods, standard anti- $k_t(0.5)$  calorimeter jets and pile up corrected anti- $k_t(0.5)$  calorimeter jets.

### 5.3 Level-1 Trigger Pile-up Mitigation

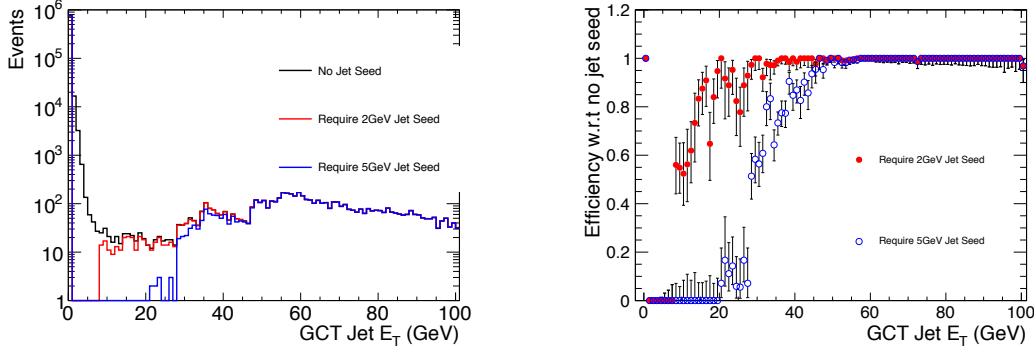
Whilst we have seen that the offline performance of the Level-1 hadronic triggers can be maintained when raising the trigger thresholds to deal with increased rate, when switching to pile up corrected offline objects. Figure 5.14 shows the trigger cross section as a function of instantaneous luminosity for the L1\_HTT150 trigger, which requires  $H_T > 150$  GeV. However beyond a certain point raising thresholds causes a loss of performance. In this section we look at a method to reduce the effects of pile up hadronic Level-1 triggers, by making an addition to the Level-1 jet finding algorithm.

In Section 5.1 the Level-1 jet clustering algorithm was described. The proposed change was to add a requirement that the seeding region has a direct energy threshold, in addition to the equality relations that are set up. The effects of applying a 2 GeV or a 5 GeV threshold are studied. This threshold is on the raw, uncorrected energy of the trigger towers and effects all Level-1 jets. The impact will be seen in the Level-1 jet triggers which use corrected energy and Level-1  $H_T$  and  $\#_T$  which are formed from uncorrected jets. The aim is to remove the events which are accepted due to pile up, but not to remove physics events.

The triggers most effected by this change are the energy sum triggers as they sum many jets of low threshold, where as the single object triggers are already cutting on high  $E_T$  objects.

Figure 5.12(a) shows the internal GCT uncorrected jet energy spectrum in high pile up conditions, taken with the L1\_SingleMu pass though triggers. The three histograms are for; no application of jet seed threshold in black, where there are many low  $E_T$  jets; In red a 2 GeV seed requirement is made, the effect is to cut out all jets below 2 GeV and cut out jets with an energy up to approximately 35 GeV of uncorrected energy; The blue histogram shows the jet energy spectrum after applying a 5 GeV seed threshold, the effect is to remove all jets below 5 GeV and to cut out jets with energy up to 55 GeV. Figure 5.12(b) shows the efficiency with respect to the no seed sample for the two test seed thresholds. The removal of jets in the low energy region of the  $E_T$  spectrum is where the advantage of applying a seed threshold is seen over simply raising the trigger thresholds, or raising the threshold of jets to be included in the Level-1  $H_T$  or  $\#_T$  calculation.

To quantify the effects of the addition of the jet seed a low pile up sample, where the effects are expected to be small, is studied in terms of rate reduction and efficiency change. The dedicated high pile up fill is then studied in terms of rate reduction, due to



(a) GCT internal uncorrected jet  $E_T$  distributions for the same events with a 0, 2 or 5 GeV seed requirement. (b) Efficiency of applying a requirement of 2 or 5 GeV with respect to no requirement.

**Figure 5.12:** Effect of requiring a jet seed threshold on GCT internal jets.

the limited sample size of the high pile up fill the change in efficiency on this sample is not studied. However due to the addition of energy from the secondary pile up interactions the change in efficiency in the low pile up sample is the worse case scenario.

Table 5.1 details the rate reduction with respect to the 0 GeV seed threshold for seed thresholds of 2 GeV and 5 GeV for three example triggers, these are:

- L1\_SingleJet50, which requires at least one jet with  $E_T > 50$  GeV with in  $|\eta| < 3.0$ ;
- L1\_QuadJet38, which requires 4 jets with  $E_T > 38$  GeV with in  $|\eta| < 3.0$ ;
- L1\_HTT100, which requires that Level-1  $H_T > 100$  GeV.

The rate of L1\_SingleJet50 is not effected by the requirement of a 2 GeV seed threshold and is reduced by 15% when a 5 GeV seed requirement is made. The L1\_QuadJet38 trigger rate is reduced by the same amount as the single jet trigger, under low pile up conditions for both seed thresholds. L1\_HTT100 sees a 2% rate reduction when requiring a 2 GeV seed threshold and a 3% reduction in rate when requiring a 5 GeV seed.

Table 5.2 shows the rate reduction under high pile up conditions with respect to the 0 GeV seed threshold requirement, for the same three example triggers as in the low pile up case. The rate of L1\_SingleJet50 is not reduced when making a 2 GeV seed requirement, when making a 5 GeV seed requirement the single jet 50 GeV rate is reduced by 30%. The rate of L1\_QuadJet38 is reduced by 30% when requiring a 2 GeV



**Table 5.1:** Summary of rate reduction during low pile up conditions.

Trigger	% rate reduction with a 2GeVrequirement	% rate reduction with a 5GeVrequirement
L1_HTT100	$3 \pm 11\%$	$3 \pm 11\%$
L1_QuadJet38	$0 \pm 0\%$	$15 + 6 - 8\%$
L1_Jet50	$0 + 0 - 12\%$	$15 + 9 - 15\%$

**Table 5.2:** Summary of rate reduction during high pile up conditions.

Trigger	% of rate taken with 2GeVrequirement	% of rate taken with 5GeVrequirement
L1_HTT100	$40 \pm 5.7\%$	$99 + / - 50\%$
L1_QuadJet38	$30 \pm 20\%$	$40 + 22 - 24\%$
L1_Jet50	$0 + 7 - 0\%$	$30 + 10 - 12\%$

seed and by 40% when requiring a 5 GeV seed. The rate of L1\_HTT100 is reduced by 40% when requiring a 2 GeV seed threshold and when requiring a 5 GeV seed threshold the rate is reduced by  $\approx 99\%$ , however the statistical error on this prediction is large.

### 5.3.1 Effect on trigger efficiency

Section 5.3 shows that requiring a jet seed threshold substantially reduces the trigger acceptance rate at in high pile up conditions.

However the aim of requiring a jet seed is to reduce rate, but not at the cost of physics. In this section we look at the effects of requiring a seed threshold, whilst requiring some loose, generic offline selection on the hadronic objects.

The change in efficiency is measured under low pile up conditions where the least extra energy added to the event. This gives a worse case estimate of the effect of requiring a jet seed on the offline efficiency.

Each offline reconstructed calorimeter jet must adhere to the following quality criteria:

- Pass loose calorimeter ID;
- $p_T \geq 30$  GeV;

- $|\eta| \leq 3.0$ ;
- Matched to a Level-1 jet with  $\Delta R \leq 0.5$ .

Where loose calorimeter ID is defined as; Electro-Magnetic fraction  $> 0.01$ , fraction of energy in the Hybrid Photo Diodes  $< 0.98$  and the number of n90hits  $> 1$ .

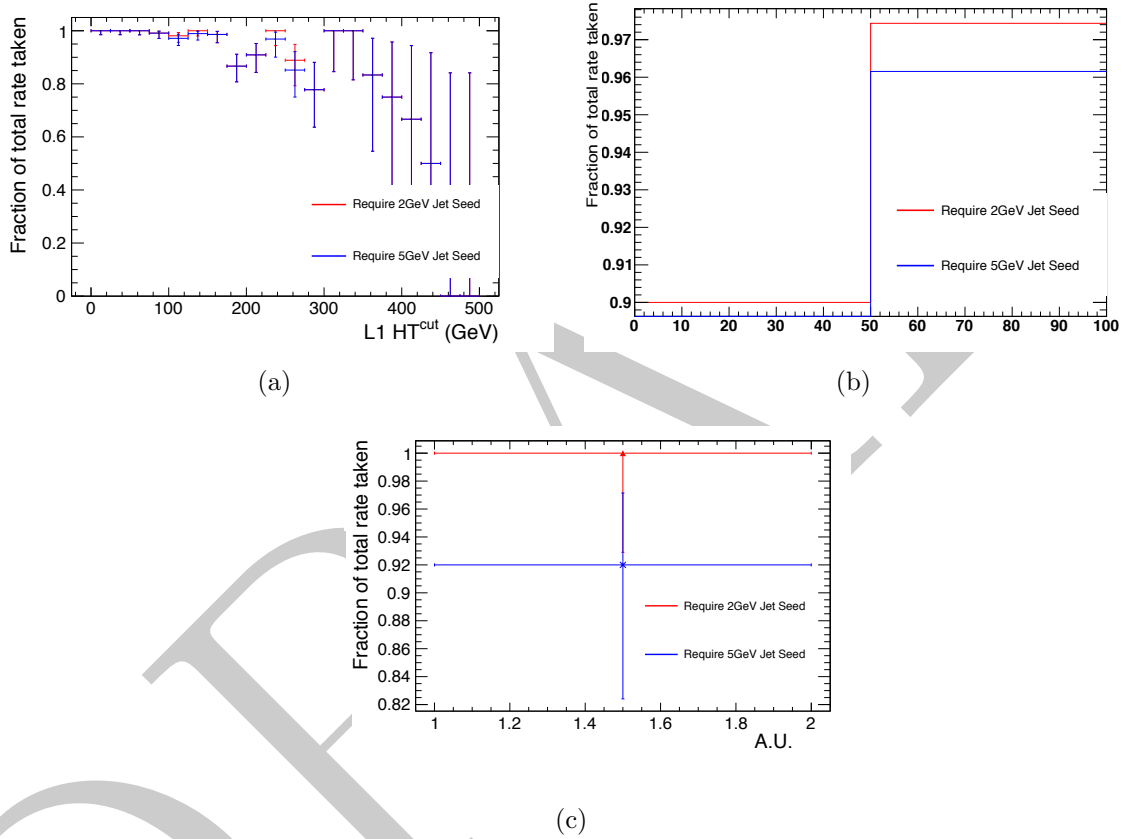


**Figure 5.13:** Efficiency reductions for various Level-1 algorithms when applying a 2 or 5 GeV seed tower requirement, in low pile up conditions. Figure (a) shows the efficiency reduction for  $H_T$  triggers at low pile up in cut steps of 25 GeV. Figure (b) shows the efficiency reduction for jets with in  $|\eta| < 3$ . and  $p_T > 50$  GeV. Figure (c) show the efficiency reduction for a quad jet trigger, with jet  $|\eta| < 3$ . and  $p_T > 38$  GeV.

**Efficiency of  $H_T$  Triggers** Figure 5.13(a) shows the acceptance reduction after applying the two jet seed thresholds. The distribution is the cumulative number of events passing a cut of  $L1HT^{cut}$  in bins of 25 GeV. Due to  $H_T$  being the scalar sum of the jet  $p_T$ 's in the event the value of Level-1  $H_T$  is reduced as jets are removed from the calculation. To preserve efficiency the Level-1 trigger threshold will have to be reduced. When comparing to the high pile up rate reduction in table 5.2 it is shown that the trigger

1 rate can be reduced by  $\approx 20\%$  when requiring a 2 GeV seed threshold and reduced by  
 2  $\geq 99\%$  when requiring a 5 GeV seed threshold, for a trigger threshold of 100 100 GeV.

3 **Efficiency of Jet Triggers** Figure 5.13(b) shows the change in acceptance of jets in  
 4 low pile up conditions when the two seed thresholds are required. The effect is on the  
 5 order of a few percent for each of the thresholds. Requiring a 2 GeV seed reduces the  
 6 efficiency for jets above 50 GeV by  $\approx 2.5\%$ , whilst requiring a 5 GeV seed reduces the  
 7 efficiency of the same jets by  $\approx 4\%$ .

8 **Efficiency of MultiJet Triggers** Figure 5.13(c) shows that the effect of requiring a  
 9 seed threshold of 2 GeV has no effect on the efficiency of the quad jet 38 GeV trigger  
 10 and requiring a seed threshold of 5 GeV reduces the efficiency of the quad jet 38 trigger  
 11 by 8%. The change in rate is dramatic in high pile up conditions where for a 2 GeV seed  
 12 threshold the rate is reduced by  $\approx 30\%$  and by  $\approx 40\%$  when requiring a 5 GeV seed.  
 13 However it is to be noted that the sample where this measurement has been made is of  
 14 limited size, inferring a reasonably large statistical uncertainty.

### 15 5.3.2 Summary

16 The effects of requiring a jet seed have been studied using the Level-1 trigger emulator on  
 17 high and low pile-up samples. The studies show that requiring a jet seed of 5 GeV greatly  
 18 reduces the rate of the  $H_T$  and Multi Jet triggers in high pile up conditions, whilst not  
 19 adversely effecting the data taking efficiency of these triggers.

20 The cross section of L1\_HTT150 has been measured with and with out the addition  
 21 of a jet seed threshold of 5 GeV as shown in Figure 5.14. Ideally the trigger cross section  
 22 would be independent of the instantaneous luminosity and pile up, Figure 5.14 shows  
 23 that the addition of a 5 GeV seed threshold reduces the dependance on instantaneous  
 24 luminosity of the trigger cross section.

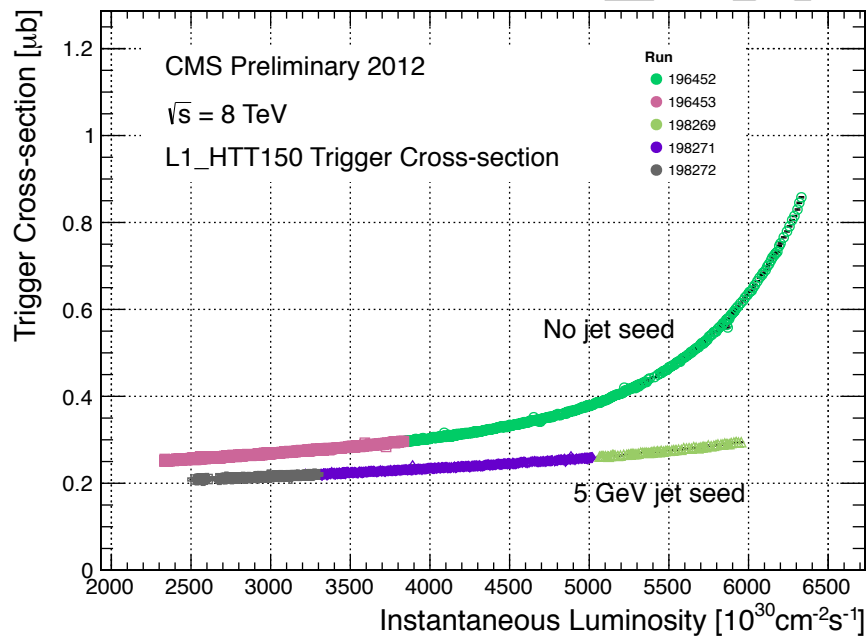


**Figure 5.14:** Trigger cross section as a function of number of pile up interactions. Showing that applying a 5 GeV jet seed threshold dramatically reduces the dependence of cross section on the instantaneous luminosity.

## Chapter 6

- <sub>1</sub> High level triggers for the  $\alpha_T$
- <sub>2</sub> analysis.

# Chapter 7

## The $\alpha_T$ analysis

In this chapter we discuss the main analysis performed as the subject of this thesis. For the theoretical motivations of this search please see Chapter 2. The analysis is based on the full 2011 data set which is made up of  $5 \text{ fb}^{-1}$  of 7 TeV data. However  $5 \text{ fb}^{-1}$  of the 2012 8 TeV is looked at to measure the performance of the upgraded  $\alpha_T$  HLT paths.

### 7.1 The Problem

If Supersymmetry or some other beyond the standard model theory is to provide a yet undiscovered dark matter candidate, it is predicted that this candidate will interact via the weak nuclear force only. This gives a decay topology involving missing energy in the form of the dark matter particle escaping the detector. Due to the nature of interactions at the L.H.C, these particles would be produced at the end of a decay chain of heavy particles that interact strongly, giving a final topology involving hadronic objects which are classified as jets for the purpose of analysis and missing energy. There are several standard model processes that mimic this final state.

By far the largest of these backgrounds comes from QCD multi jet events where fake missing energy is introduced either from failures in reconstruction, or stochastic fluctuations in the calorimeter systems. **FIXME: expand on this -  $E/\sqrt{E}$  has non gaussian tails. Figures of jets falling below threshold, missed jets etc. probably from some jet-met paper.** However due to the theoretical errors on the QCD production cross section predicting the number QCD background events from Montecarlo simulation is not possible. A secondary QCD background also exists, where due to the requirement of a jet  $E_T$  threshold, multiple jets fall under threshold by a few

GeV, this causes a balanced event to look unbalanced as the jets under threshold are no longer considered. It is these events that  $\alpha_T$  is designed to remove.

The second major background comes from standard model electro-weak decays and is irreducible as the final states involve real missing energy, from neutrinos. The electro-weak decays that form the back ground are  $W \rightarrow \tau\nu + \text{Jets}$ , where the  $\tau$  is reconstructed as a jet, or the lepton fails the identification required for the dedicated lepton vetoes,  $Z \rightarrow \nu\bar{\nu} + \text{Jets}$  is completely irreducible. These are generally di-jet topologies. At higher jet multiplicities top quark production followed by semi-leptonic top decay accounts of the largest background. These backgrounds are predicted using a well understood control sample this is fully explained in Section 7.6.

The final background source is that introduced by detector failure or electronic noise induced by the movement of the L.H.C proton beam. Approximately 1% of the ECAL read out is not available in offline event reconstruction, this provides a source of fake missing energy.

## 7.2 The $\alpha_T$ variable.

$\alpha_T$  is inspired by Ref [12] and was expanded to transverse multi jet topologies by members of the CMS collaboration in Refs [7, 8]. The purpose is to provide a variable that can be cut on to eliminate QCD from the final selection. To do this the inherent balance of the QCD system is exploited.

For di-jet systems  $\alpha_T$  is defined as:

$$\alpha_T = \frac{E_T^{j_2}}{M_T} \quad (7.1)$$

where  $E_T^{j_2}$  is the transverse energy of least energetic of the two jets and  $M_T$  is defined as:

$$M_T = \sqrt{\left(\sum_{i=1}^2 E_T^{j_i}\right)^2 - \left(\sum_{i=1}^2 p_x^{j_i}\right)^2 - \left(\sum_{i=1}^2 p_y^{j_i}\right)^2} \quad (7.2)$$

For a perfectly measured di-jet system with  $E_T^{j_1} = E_T^{j_2}$ , where the jets are opposite in  $\phi$   $\alpha_T = 0.5$ , for events with back to back jets where one is miss-measured  $\alpha_T < 0.5$ . However the majority of signals predict many jets in the final state.  $\alpha_T$  can be generalised to work with n-jets in the following way. The variables  $H_T$ ,  $\cancel{H}_T$  and  $\Delta H_T$  are constructed:

$$H_T = \sum_{i=0}^{n \text{ jets}} E_T^{jet_i} \quad (7.3)$$

$$\cancel{H}_T = \left| \sum_{i=0}^{n \text{ jets}} \vec{p}_T^{jet_i} \right| \quad (7.4)$$

- 1 for jets above some predefined threshold  $E_T$  which is common for all jet based quantities.
- 2 The multi jet system is reduced to a pseudo di-jet system by forming two large jets. The
- 3 individual jet  $E_T$ 's are summed, with the final configuration being chosen to have the
- 4 minimum difference in energy ( $\Delta H_T$ ) between the pseudo jets. This simple clustering
- 5 criteria provides the best separation between miss-measured events and those with real
- 6  $\cancel{E}_T$ .

$\alpha_T$  is then defined as:

$$\alpha_T = \frac{H_T - \Delta H_T}{2\sqrt{H_T^2 - \cancel{H}_T^2}} \quad (7.5)$$

- 7 Figure 7.1 shows the  $\alpha_T$  distribution for both data and simulated background samples.
- 8 The QCD multi jet background is negligible above an  $\alpha_T$  value of 0.55, where as the
- 9 standard model processes which involve real  $\cancel{E}_T$  exist at all possible values of  $\alpha_T$ . Values
- 10 of  $\alpha_T$  in the range  $0.5 < \alpha_T < 0.55$  arise in multi jet QCD due to jets falling below
- 11 threshold or large stochastic fluctuations. It is to be noted that the discrepancy between
- 12 data and simulation for  $\alpha_T \leq 0.55$  is due to no trigger emulation being applied to the
- 13 simulated background samples.

### 14 7.3 Event selection

- 15 In order to select events for the hadronic signal sample and the muon and photon control
- 16 samples a common set of section cuts is defined. In this section the objects are defined
- 17 as are the flow of the analysis cuts and filters.



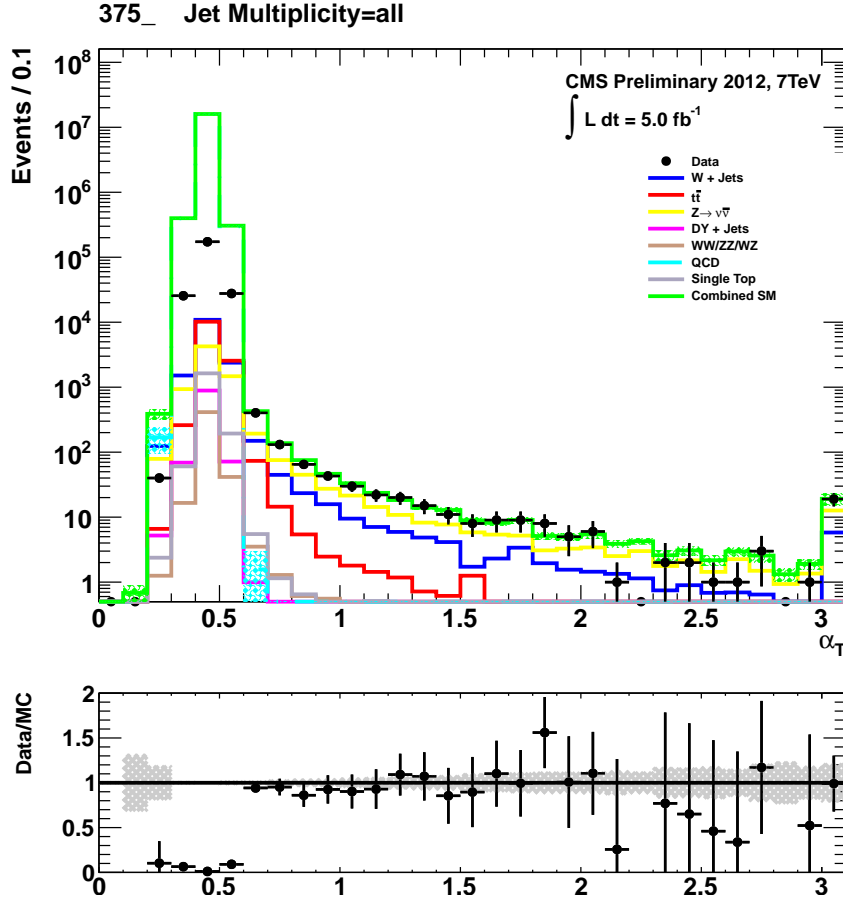


**Figure 7.1:**  $\alpha_T$  distribution for background and data. Trigger emulation is not applied in the simulated background which leads to the discrepancy in the region  $\alpha_T \leq 0.55$ . The QCD multi-jet background is reduced to less than one event.

**Preselection of hadronic objects** Jets are created by running the anti- $k_t(0.5)$  jet clustering algorithm[4] over the calorimeter towers. The jets have their raw energies corrected based on their position and momentum to establish a uniform relative response in  $\eta$  and a calibrated absolute response in transverse energy  $E_T$ , with an associated uncertainty of between 2% and 4% dependant on  $E_T$  and  $\eta$ [5]. Jets considered in the analysis are required to have  $E_T > 50$  GeV, the highest  $E_T$  jet in the events is required to be within tracker acceptance ( $-\eta < 2.5$ ) and the sub leading jet is required to have  $E_T > 100$  GeV. The quantities  $H_T$  and  $\#_T$  are then formed from these jets.

The common selection cuts and filters consist of:

- **All detector subsystems on**, Compact Muon Solenoid (C.M.S) in “Physics Declared” mode and all physics object groups have certified the runs and luminosity

sections. This removes any events where the sub-detectors were in an error state or events from before the tracker was switched to high voltage mode.

- **P.K.A.M (Previously Known As Monsters) filter**, these events are caused by beam-gas interactions close to C.M.S, which cause a shower of particles to enter the pixel detector along the beam line, resulting in a large proportion of the pixel detector to record hits.
- **Vertex Selection** requires at least one non-fake vertex with at least four associated tracks, within a cylinder of radius 2 cm and length 48 cm, centred at  $Z = 0$  of the C.M.S detector.
- **Hadronic barrel and end-cap noise filter**, this filter removes events where strips of towers in the hadronic calorimeters record energy from electrical noise, mimicking large, unbalanced energy deposits.
- **Vertex  $p_T / H_T > 0.1$** , removes events where the sum of the  $p_T$  of all tracks from all good vertices is less than 10% of the energy deposited by jets in the calorimeters. This cut is designed to remove events with tracking failure, which would otherwise pass the calorimeter only event quality requirements.
- **Masked ECAL channel filter**: Approximately 1% of the ECAL crystals are masked, or have read out failure. To avoid selecting events with large energy miss measurement, a topological cut was devised. The first step is to calculate  $\Delta\phi^*$  for each jet ( $\vec{j}$ ) in the event, where:

$$\Delta\phi^* = \Delta\phi\left(\vec{E}_T + \vec{j}, \vec{j}\right). \quad (7.6)$$

Which gives a measure of the miss measurement of a jet, if  $\Delta\phi^*$  is small, the missing energy points along the jet in the  $\phi$  direction. By selecting the miss measured jet, full position information is preserved. If any jet has  $\Delta\phi^* < 0.5$ , the number of masked ECAL crystals with in  $\Delta R < 0.3$  are summed, if there are more than 10 masked crystals adjacent to the jet, the event is vetoed.

- **$R_{miss} < 1.25$** : The total hadronic energy in an event is required to be greater than 275 GeV which is well above the transverse energy threshold of 50 GeV for each jet. However several jets falling below this threshold can sum to a significant quantity of ignored energy. This is shown in Figure 7.2, here the missing energy calculated from jets in the range  $10 \text{ GeV} < E_T < 50 \text{ GeV}$  is shown, whilst requiring that  $\cancel{E}_T$

$< 20$  GeV. This shows that for a well balanced event the jets below threshold can carry greater than 100 GeV of ignored energy.  $R_{miss}$  is defined as  $\cancel{E}_T/\cancel{E}_T$  and can be used to single out events where the inclusion of lower momentum jets does significantly improve the balance of the event.

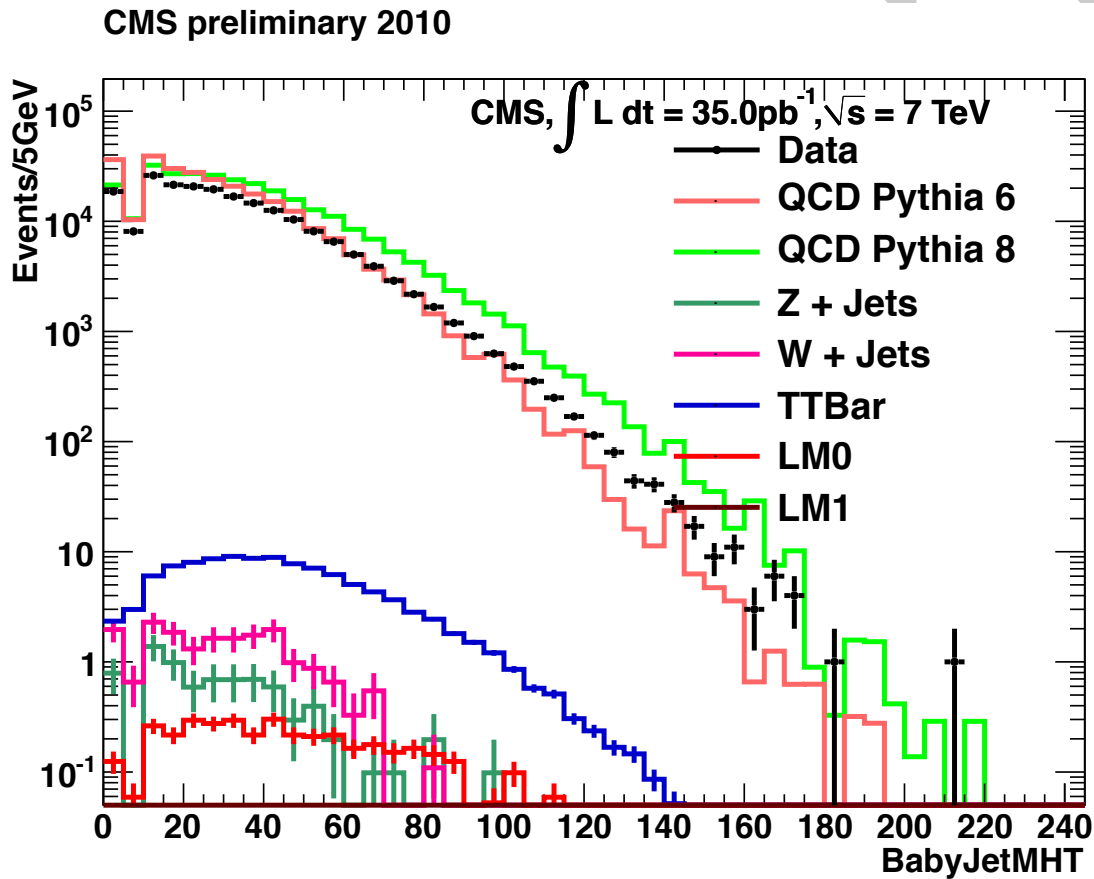


**Figure 7.2:**  $\cancel{E}_T$  from jets with  $10 \text{ GeV} < E_T < 50 \text{ GeV}$  in events with  $H_T > 350 \text{ GeV}$  and  $\cancel{E}_T < 20 \text{ GeV}$  in  $35 \text{ pb}^{-1}$  of data.

## 7.4 High Level triggers for the $\alpha_T$ analysis

The CMS trigger system has been discussed in detail in Section 3.1 and Chapter 5, however details of analysis specific trigger paths were not discussed. During 2011 the first  $\alpha_T$  specific trigger was designed and deployed online. The trigger was then upgraded for the higher luminosity and energy conditions of the 2012 data taking period.

The trigger takes advantage of cutting on two variables,  $H_T$  and  $\alpha_T$  at low  $H_T$  a high  $\alpha_T$  value cuts the trigger rate, where as at high  $H_T$  where the trigger rate is lower the  $\alpha_T$  requirement can be loosened.

Due to the scaling of jet thresholds in the lowest offline  $H_T$  bins as detailed in Section 7.3 using a fixed jet threshold would cause inefficiency in the lowest offline  $H_T$  bins. To overcome this the trigger level  $\alpha_T$  calculation is performed iteratively for all jets above a predefined threshold. This raises the total number of accepted events whilst adding the benefit of being efficient for any offline jet threshold above the minimum trigger jet threshold. The algorithm is shown in Figure 7.3.

## 7.5 2011 Trigger

Due to concerns on the time taken to perform the  $\Delta H_T$  minimisation at the trigger and time constraints enforced on trigger menu development, the first implementation calculates  $\alpha_T$  for the first 3 jets. For higher jet multiplicities the variable  $\beta_T$  is calculated.

$$\beta_T = \frac{H_T}{2\sqrt{H_T^2 - \#_T^2}} \quad (7.7)$$

this gives us the relation:

$$\alpha_T \leq \beta_T. \quad (7.8)$$

The decision flow is shown in Figure 7.3 and explained in detail below.

When a level one accept is issued the trigger bits that fired are checked, if the event fires a L1 muon trigger it is passed to the HLT muon triggers where only muon reconstruction is performed, reducing the reconstruction time. The  $\alpha_T$  triggers are seeded on the lowest threshold unscaled L1  $H_T$  trigger, during 2011 this was L1\_HTT100. Any events issuing a L1 accept and passing L1\_HTT100 undergo calorimeter jet reconstruction, the reconstruction algorithm is detailed in Section 4.1.

Once the jets have been formed the trigger filter is entered. Initially the first two jets ranked by  $E_T$ , are considered,  $H_T$  and  $\alpha_T$  are calculated, if both pass the trigger thresholds the event is accepted and the full detector read out is performed. If either  $H_T$  or  $\alpha_T$  is below threshold, the next jet in  $E_T$  order is added, if the jet collection contains

more than 3 jets then the  $\beta_T$  approximation is used. All jets in the event are added until either the event is accepted, or there are no more jets to be added above 40 GeV.

The effect of switching to the  $\beta_T$  approximation is to accept events that have missing energy due to miss-measurement, when calculating  $\alpha_T$  offline these events have values of  $\alpha_T < 0.5$ . This introduces an impurity to the trigger and costs rate for events that will not be considered in the offline analysis.

### 7.5.1 Trigger efficiency measurement

The performance of the  $\alpha_T$  trigger suit is measured with respect to a sample collected using the muon system. This allows the measurement of efficiency of both the level one seed trigger and the higher level trigger at the same time as different sub-systems are used to collect the reference and the signal triggers. This is due to the exclusive use of calorimeter jets in the  $\alpha_T$  trigger, if more complicated reconstruction methods which produce an event hypothesis were used, muons would at HLT level only be considered as jets. Where as during calorimeter only reconstruction, muons are not considered and the  $p_T$  of any muons in an event is viewed as missing energy.

## 7.6 Electro-Weak background prediction

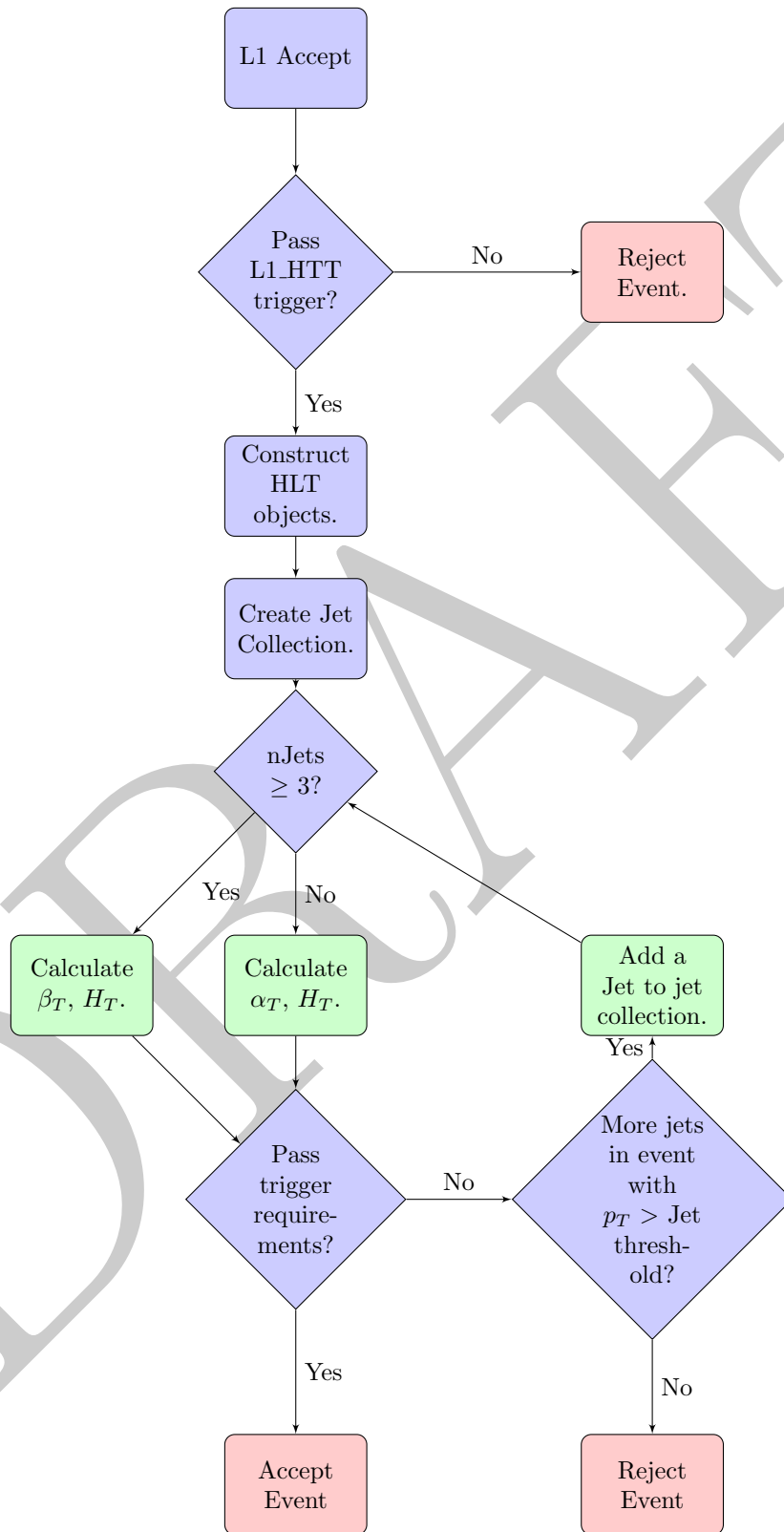


**Figure 7.3:** Flow chart representing the steps taken to make a trigger decision using the  $\alpha_T$  trigger algorithm.

## Chapter 8

### <sub>1</sub> Conclusion

DRAFT



# Bibliography

- [1] T Åkesson. The ATLAS experiment at the CERN Large Hadron Collider - CERN Document Server. *Particles*, 1999.
- [2] B Alessandro, F Antinori, J Belikov, and C Blume. ALICE: Physics performance report, volume II. *Journal of Physics G: Nuclear and Particle Physics*, January 2006.
- [3] Michael Benedikt, Paul Collier, V Mertens, John Poole, and Karlheinz Schindl. *LHC Design Report*. CERN, Geneva, 2004.
- [4] M Cacciari, G Salam, and G Soyez. The anti-kt jet clustering algorithm. *Journal of High Energy ...*, January 2008.
- [5] Serguei Chatrchyan and others. Determination of Jet Energy Calibration and Transverse Momentum Resolution in CMS. *arXiv*, 6:P11002, 2011.
- [6] CMS Collaboration. The Trigger and Data Acquisition Project Technical Design Report, Volume 1, The Level-1 Trigger. *CERN/LHCC 2000-038, CMS TDR 6.1*, 2000.
- [7] CMS Collaboration. SUSY searches with dijet events. Technical report, 2008.
- [8] CMS Collaboration. Search strategy for exclusive multi-jet events from supersymmetry at CMS. Technical report, 2009.
- [9] M Friedl, N Frischauf, T Bauer, T Bergauer, W Waltenberger, A R Knapitsch, C Imler, I Kratschmer, W Treberer-treberspurg, B Rahbaran, V Innocente, T Camporesi, S Gowdy, L Malgeri, A Marchioro, L Moneta, W Weingarten, M Giunta, M Rovere, A Bonato, A C Spataru, S Zhang, A Perieanu, N Heracleous, H K V Reithler, B Philipps, M K Merschmeyer, C A Heidemann, H Geenen, Y Kuessel, E Kuznetsova, J Olzem, A Bethani, L Calligaris, R Walsh bastos rangel, T M M Dorland, G Quast, A H Dierlamm, I Katkov, R M Ulrich, F M H Stober, C Barth, X Mol,

A Kornmayer, F Matorras, A Calderon tazon, A Lopez garcia, J A Brochero cifuentes, M J Bercher, M Haguenauer, Y Sirois, C M Mironov, P Depasse, L Sgandurra, G P Heath, Z Meng, D A Hartley, N I Geddes, S Quinton, I R Tomalin, K Harder, V B Francis, Z Zhang, T Gerals, D Loukas, I Topsis giotis, G Bencze, S T Hernath, I Szeberenyi, S Banerjee, S Singh, A Colaleo, G P Maggi, M Maggi, F Loddo, R Campanini, I D'antone, C Grandi, L Guiducci, M Gulmini, S Fantinel, P Merid-  
iani, K K Joo, S Song, J Rhee, E Won, M Jo, H Kim, D H Kim, G N Kim, J E Kim, T Son, W M Dominik, K Bunkowski, J C Rasteiro da silva, J Varela, A Alves, V Sulimov, A Vorobyev, V Murzin, S Lukyanenko, G Mesyats, V Postoev, A Pashenkov, A Solovey, S Troitsky, N Lychkovskaya, G Safronov, A Fedotov, K Olimov, M Fazilov, A Umaraliev, I Dumanoglu, N M Bakirci, C Dozen, M Zeyrek, M Yalvac, S Ozkorucuklu, K Sevim, Y Chang, W T Lin, S Bahinipati, K A Biery, E E Gottschalk, K Maeshima, T Kramer, S W L Kwan, S J Murray, L Taylor, N Mokhov, J M Marraffino, S Mrenna, V Yarba, B Banerjee, V D Elvira, D C Hare, B Holzman, F X Yumiceva del pozo, W Dagenhart, C L Dumitrescu, S C Ryu, B J Kilminster, J K Adelman-mc carthy, V E Bazterra, I Bucinskaite, P E Karchin, J R Incandela, M D'Alfonso, R Rossin, C A West, J L Gran, G Zilizi, P P Raics, A Bhardwaj, M Naimuddin, A Kumar, N Smiljkovic, C P De oliveira martins, M Petek, A Vercosa custodio, E J Tonelli manganote, M T Narjanen, P Graehling, F Blekman, J M Keaveney, S Blyweert, N van Remortel, X J Janssen, D Druzhkin, M Bansal, A Aleksandrov, M F Shopova, T R Fernandez perez tomei, C Krug, A A Shinoda, T V Rohe, P Arce, M Daniel, J J Navarrete marin, I Redondo fernandez, A Guirao elias, J Santaolalla camino, J Lottin, P Gras, F Kircher, B Levesy, A Payn, A K Nayak, V Bhatnagar, C Randieri, M Bruzzi, O Starodubtsev, A Tropiano, D Piccolo, C Sciacca, S Meola, A Saccomanno, M Esposito, P Azzi, E Conti, S Lacaprara, M Margoni, M Sgaravatto, N Pozzobon, P Torre, B Checcucci, L Fanò, S Taroni, A Lucaroni, F Romeo, G Bagliesi, M A Ciocci, A Giassi, T Boccali, S Arezzini, A Rizzi, G Broccolo, D Dattola, C Mariotti, A Ballestrero, E Camacho-Pérez, R Magaña-Villalba, J Martínez-Ortega, M Górski, G Wrochna, M J Bluj, A Zarubin, M Nozdrin, V Ladygin, A Golunov, A Sotnikov, N Evdokimov, I Lokhtin, A Ershov, N Tyurin, S Akimenko, V Talov, N Belikov, A Ryazanov, G W Hou, Y Chao, J Alwall, X Shi, D R Wood, D C Baumgartel, J Zhang, P D Luckey, K C Sumorok, G Gomez ceballos retuerto, S H Jaditz, G S Stephans, T Ma, P J Lehtonen, M H Chan, I J Moulton, R A Ofierzynski, A Pozdnyakov, B L Pollack, P B Padley, A H Adair, W J Clarida, E Tiras, G Cerizza, M Pieri, V A Sharma, M W Lebourgeois, M Norman, F Golf, M J Murray, J L S Bowen, K Buterbaugh, M Sharma, J Bunn,

- 1 H Newman, M Gataullin, M Spiropulu, J Veverka, S D Thomas, K J Rose, S M  
2 Panwalkar, A Calamba, Z Xie, J S Werner, A M Zuranski, A Ferapontov, E M Laird,  
3 G Kukartsev, Z Mao, S J Wimpenny, S Gleyzer, M G Weinberg, V Veeraraghavan,  
4 and J... Bochenek. CMS - The Compact Muon Solenoid. January 1996.
- 5 [10] J Marrouche and others. Commissioning the CMS Global Calorimeter Trigger. *CMS*  
6 *IN*, 2010/029, 2010.
- 7 [11] J Rademacker. LHCb: Status and Physics Prospects. *Arxiv preprint hep-ex*, January  
8 2005.
- 9 [12] Lisa Randall and David Tucker-Smith. Dijet Searches for Supersymmetry at the  
10 LHC. *arXiv*, hep-ph, January 2008.
- 11 [13] C Wulz. The CMS experiment at CERN. *cdsweb.cern.ch*.